Crystal structure of post-perovskite-type CaIrO₃ reinvestigated: new insights into atomic thermal vibration behaviors

**Akihiko Nakatsuka,ª* Kazumasa Sugiyama,ᵇ Akira Yoneda,ᶜ Keiko Fujiwaraª and Akira Yoshiasaᵈ**

ªGraduate School of Science and Engineering, Yamaguchi University, Ube 755-8611, Japan, ᵇInstitute for Materials Research, Tohoku University, Sendai 980-8577, Japan, ᶜInstitute for Study of the Earth's Interior, Okayama University, Misasa 682-0193, Japan, and ᵈGraduate School of Science and Technology, Kumamoto University, Kumamoto 860-8555, Japan. *Correspondence e-mail: tuka@yamaguchi-u.ac.jp

Single crystals of the title compound, the post-perovskite-type CaIrO₃ [calcium iridium(IV) trioxide], have been grown from a CaCl₂ flux at atmospheric pressure. The crystal structure consists of an alternate stacking of IrO₆ octahedral layers and CaO₈ hendecahedral layers along [010]. Chains formed by edge-sharing of IrO₆ octahedra (point-group symmetry 2/m..) run along [100] and are interconnected along [001] by sharing apical O atoms to build up the IrO₆ octahedral layers. Chains formed by face-sharing of CaO₈ hendecahedra (point-group symmetry m2m) run along [100] and are interconnected along [001] by edge-sharing to build up the CaO₈ hendecahedral layers. The IrO₆ octahedral layers and CaO₈ hendecahedral layers are interconnected by sharing edges. The present structure refinement using a high-power X-ray source confirms the atomic positions determined by Hirai et al. (2009) [Z. Kristallogr. **224**, 345–350], who had revised our previous report [Sugahara et al. (2008). Am. Mineral. **93**, 1148–1152]. However, the displacement ellipsoids of the Ir and Ca atoms based on the present refinement can be approximated as uniaxial ellipsoids elongating along [100], unlike those reported by Hirai et al. (2009). This suggests that the thermal vibrations of the Ir and Ca atoms are mutually suppressed towards the Ir···Ca direction across the shared edge because of the dominant repulsion between the two atoms.

1. Chemical context

The orthorhombic perovskite-type MgSiO₃, the dominant constituent in the Earth's lower mantle, is now believed to undergo the phase transition to the so-called 'post-perovskite-type structure', associated with the D″ seismic discontinuity, at 125 GPa and 2500 K (Murakami et al., 2004; Tsuchiya et al., 2004; Oganov & Ono, 2004; Iitaka et al., 2004; Mao et al., 2004; Ono & Oganov, 2005; Wentzcovitch et al., 2006; Shieh et al., 2006). Since the discovery of the post-perovskite-type MgSiO₃, several orthorhombic $A^{2+}B^{4+}O_3$ perovskite-type compounds have been found to transform into the post-perovskite-type structure under high pressure and high temperature (Kojitani et al., 2007; Yamaura et al., 2009; Tateno et al., 2010). Meanwhile, CaIrO₃ is known to be one of the few post-perovskite-type compounds stable at ambient conditions (Rodi & Babel, 1965; McDaniel & Schneider, 1972). The post-perovskite-type CaIrO₃ has attracted much attention in the field of Earth science as an excellent low-pressure analogue of the post-perovskite-type MgSiO₃ (see, for example, Niwa et al., 2007; Tsuchiya & Tsuchiya, 2007; Yoneda et al., 2014).

The crystal structure of the post-perovskite-type CaIrO₃ was first proposed by Rodi & Babel (1965) on the basis of a

OPEN ACCESS

research communications
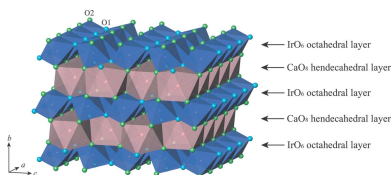
single-crystal X-ray diffraction experiment, but incorrect atomic positions were reported. Recently, we have successfully grown single crystals of the post-perovskite-type $CaIrO_3$ and refined the crystal structure of this compound on the basis of single-crystal X-ray diffraction data measured using a sealed X-ray tube (40 kV, 30 mA) as the radiation source (Sugahara *et al.*, 2008). However, the measured intensity data were rather weak and their accuracy was rather low, because thin needle-like crystals were obtained and the selected crystal for the intensity measurements had a poor grade of crystallinity. This resulted in rather large reliability indices [$R(F) = 0.064$, $wR(F) = 0.065$ for 377 reflections] and in structural parameters with rather large uncertainties. In particular, the resulting displacement ellipsoids were unusually elongated or flattened. Subsequently, Hirai *et al.* (2009) reinvestigated the crystal structure of the post-perovskite-type $CaIrO_3$ by single-crystal X-ray diffraction and conducted structure refinements for two different crystals using two different types of diffractometers. The two independent refinements showed convergent results with much better reliability indices [$R(F^2) = 0.013$, $wR(F^2) = 0.031$ for 365 reflections; $R(F^2) = 0.007$, $wR(F^2) = 0.008$ for 149 reflections] and structural parameters with reasonably smaller uncertainties. Consequently, Hirai *et al.* (2009) concluded that the displacement ellipsoids had no significant anisotropies in contradiction to our previous report (Sugahara *et al.*, 2008), but provided no further details of the atomic thermal vibration behaviors. Their X-ray diffraction experiments were conducted under the operating conditions of $2\theta_{max} = 80°$ at 45 kV/40 mA for one crystal and $2\theta_{max} = 55°$ at 50 kV/85 mA for the other crystal. These operating conditions with a low X-ray power and a relatively low $2\theta_{max}$ value may be insufficient for the determination of reliable atomic displacement parameters (ADPs).

In the present study, the crystal structure of the post-perovskite-type $CaIrO_3$ was reinvestigated on the basis of single-crystal X-ray diffraction data measured over a much wider 2θ range using a high-power rotating-anode X-ray generator (60 kV, 250 mA). Special attention to exclude the influence of multiple scattering effects and secondary extinction effects on ADPs was paid as far as possible during data reduction and structure refinement procedures, as will be described in Section 5. On the basis of the resulting structural parameters, the validity of the crystal structure proposed by Hirai *et al.* (2009) is examined and the detailed atomic thermal vibration behaviors are discussed.

Table 1
Selected bond lengths (Å).

Ca—O1^i	2.333 (3)	Ir—O1	1.9722 (15)
Ca—O2^i	2.460 (2)	Ir—O2^{iii}	2.0488 (18)
Ca—O2^{ii}	2.506 (3)		

Symmetry codes: (i) $x - \frac{1}{2}, y + \frac{1}{2}, z$; (ii) $x, -y + 1, -z + 1$; (iii) $-x - \frac{1}{2}, -y + \frac{1}{2}, z - \frac{1}{2}$.

2. Structural commentary

The post-perovskite-type phase of $CaIrO_3$ crystallizes in the space group *Cmcm*. The crystal structure consists of IrO_6 octahedral layers and CaO_8 hendecahedral layers stacked alternately along [010] (Fig. 1). The Ca and Ir atoms occupy Wyckoff positions 4c and 4a, respectively. The O atoms occupy two non-equivalent sites: O1 at Wyckoff position 4c and O2 at Wyckoff position 8f. The site symmetries are *m2m* for Ca, 2/*m*.. for Ir, *m2m* for O1 and *m*.. for O2. Ca—O and Ir—O bond lengths are listed in Table 1. In the IrO_6 octahedral layers (Fig. 2), chains of IrO_6 octahedra along [100] are formed by sharing O2···O2 edges, and these chains are interconnected along [001] by sharing the apical O1 atoms. In the CaO_8 hendecahedral layers (Fig. 3), chains of CaO_8 hendecahedra along [100] are formed by sharing O2···O1···O2 faces, and these chains are interconnected along [001] by sharing O2···O2 edges. The alternate stacking

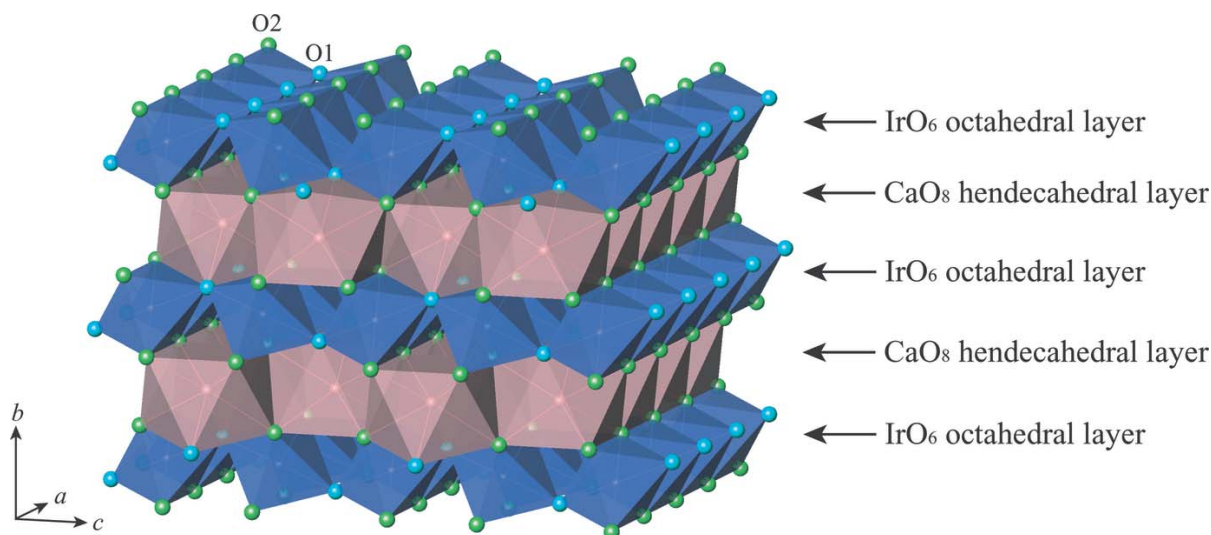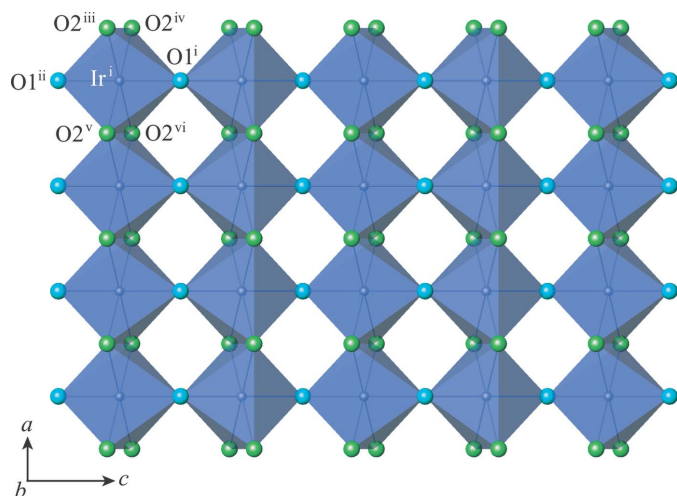**Figure 1**
Polyhedral representation of the $CaIrO_3$ post-perovskite-type structure, composed of the alternate stacking of IrO_6 octahedral layers and CaO_8 hendecahedral layers along [010].
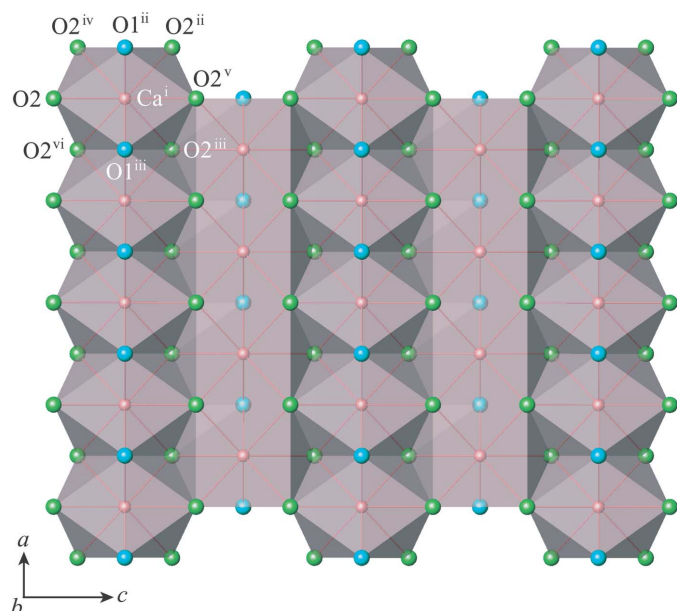
Figure 2
Polyhedral view of an IrO_6 octahedral layer projected on (010). Symmetry codes: (i) $x + \frac{1}{2}$, $y + \frac{1}{2}$, z; (ii) $x + \frac{1}{2}$, $-y + \frac{1}{2}$, $-z$; (iii) $x + 1$, $-y + 1$, $z - \frac{1}{2}$; (iv) $x + 1$, y, $-z + \frac{1}{2}$; (v) x, $-y + 1$, $z - \frac{1}{2}$; (vi) x, y, $-z + \frac{1}{2}$.

of IrO_6 octahedral layers and CaO_8 hendecahedral layers along [010] results from sharing $O1 \cdots O2$ and $O2 \cdots O2$ edges between both layers. Further details of the general description of the crystal structure are provided in our previous paper (Sugahara *et al.*, 2008).

3. Atomic thermal vibration behaviors

In the present structure refinement using a high-power X-ray source, the accuracy of the refined structural parameters was considerably improved compared with our previous report

Figure 3
Polyhedral view of a CaO_8 hendecahedral layer projected on (010). Symmetry codes: (i) x, $-y + 1$, $-z + 1$; (ii) $x + \frac{1}{2}$, $-y + \frac{1}{2}$, $z + \frac{1}{2}$; (iii) $x - \frac{1}{2}$, $-y + \frac{1}{2}$, $z + \frac{1}{2}$; (iv) $x + \frac{1}{2}$, $-y + \frac{1}{2}$, $-z + 1$; (v) x, y, $-z + \frac{3}{2}$; (vi) $x - \frac{1}{2}$, $-y + \frac{1}{2}$, $-z + 1$.
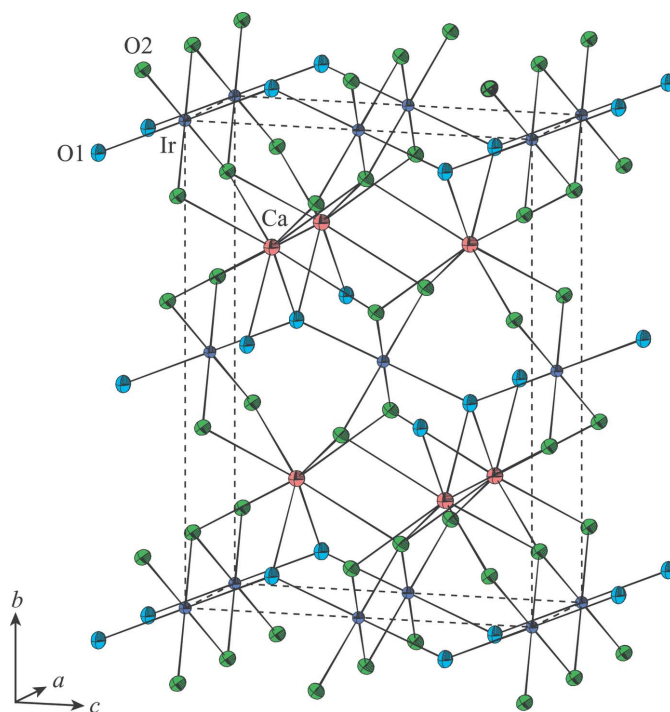
Figure 4
Unit cell of the $CaIrO_3$ post-perovskite with displacement ellipsoids drawn at the 80% probability level.

(Sugahara *et al.*, 2008), being comparable to those reported by Hirai *et al.* (2009). The resulting positional parameters also show excellent consistency with those reported by Hirai *et al.* (2009). On the other hand, the present displacement ellipsoids (Fig. 4) are different from those given by Hirai *et al.* (2009). They considered that the thermal vibrations of the Ir and Ca atoms exhibited no significant anisotropies, but in fact the reported displacement ellipsoids of both atoms were somewhat elongated parallel to the (100) plane. In contrast, the mean-square displacements (MSDs) of both atoms obtained from the present refinement are as follows: Ir, 0.00316 (5) $\mathring{A}^2$ along the shortest ellipsoid axis, 0.00319 (5) $\mathring{A}^2$ along the intermediate one and 0.00387 (6) $\mathring{A}^2$ along the longest one; Ca, 0.0055 (3) $\mathring{A}^2$ along the shortest ellipsoid axis, 0.0058 (3) $\mathring{A}^2$ along the intermediate one and 0.0065 (3) $\mathring{A}^2$ along the longest one. Here, in both atoms, the longest ellipsoid axes are just in the [100] direction and the intermediate and the shortest ones are within the (100) plane. The present results indicate that the MSDs of both atoms are significantly the largest in the [100] direction, in contradiction to the report of Hirai *et al.* (2009), although the thermal vibrations of both atoms only exhibit small anisotropies.

As understood from the MSDs shown above, the displacement ellipsoid of the Ir atom is very close to a uniaxial ellipsoid elongating along [100]. The $Ir \cdots Ca$ direction across the $O2 \cdots O2$ shared edge between the IrO_6 octahedron and CaO_8 hendecahedron is parallel to the (100) plane; hence, this direction can be considered as the direction of nearly the smallest MSD of the Ir atom although it deviates by 10.1° from the direction of the shortest ellipsoid axis. The ellipsoid axes of

Table 2
Experimental details.

Crystal data	
Chemical formula	$CaIrO_3$
M_r	280.30
Crystal system, space group	Orthorhombic, $Cmcm$
Temperature (K)	298
a, b, c (Å)	3.1466 (5), 9.8690 (16), 7.3019 (5)
V (Å^3)	226.75 (6)
Z	4
Radiation type	Mo $K\alpha$
μ (mm^{-1})	61.02
Crystal size (mm)	$0.20 \times 0.01 \times 0.01$
Data collection	
Diffractometer	Rigaku AFC7R
Absorption correction	ψ scan (North *et al.*, 1968)
T_{min}, T_{max}	0.486, 0.543
No. of measured, independent and observed [$F > 3.0\sigma(F)$] reflections	2593, 692, 438
R_{int}	0.019
$(\sin \theta/\lambda)_{max}$ (Å^{-1})	1.078
Refinement	
$R[F > 3\sigma(F)]$, $wR(F)$, S	0.011, 0.010, 1.56
No. of reflections	412
No. of parameters	20
$\Delta\rho_{max}$, $\Delta\rho_{min}$ (e Å^{-3})	1.21, −1.89

Computer programs: *WinAFC* (Rigaku, 1999), *RADY* (Sasaki, 1987), *ATOMS for Windows* (Dowty, 2000) and *publCIF* (Westrip, 2010).

the Ca atom are in the [100], [010] and [001] directions by requirements of its site symmetry, but its displacement ellipsoid can also be approximated as a uniaxial ellipsoid elongating along [100]. The Ir···Ca direction across the O2···O2 shared edge can thus be characterized also as the direction of nearly the smallest MSD of the Ca atom. These suggest that the dominant Ir···Ca repulsion across the O2···O2 shared edge suppresses the mutual thermal vibrations of both atoms towards the Ir···Ca direction. Indeed, the Ir···Ca distance [= 3.0678 (9) Å] is the shortest of the cation–cation distances [*cf.* 3.1466 (5) Å for the Ir···Ir distance across the O2···O2 shared edge between IrO$_6$ octahedra; 3.1466 (5) Å for the Ca···Ca distance across the O2···O1···O2 shared face between CaO$_8$ hendecahedra; 3.4501 (8) Å for the Ir···Ca distance across the O1···O2 shared edge between the IrO$_6$ octahedron and CaO$_8$ hendecahedron; 3.9755 (3) Å for the Ca···Ca distance across the O2···O2 shared edge between CaO$_8$ hendecahedra].

4. Synthesis and crystallization

The reagents $Ca(OH)_2$ and Ir were employed as the starting materials, and mixed together with $CaCl_2$ in the molar ratio $Ca(OH)_2$:Ir:$CaCl_2$ = 1:1:10. The mixture was heated in air at 1100 K for 8 h, and then cooled gradually to 600 K at a rate of 10 K h^{-1}. Dark reddish-brown crystals of the post-perovskite-type $CaIrO_3$ with a thin needle shape were grown from the $CaCl_2$ flux. The crystals were isolated by dissolving the solidified $CaCl_2$ melt with distilled water.

5. Refinement

A total of 2593 intensity data up to $2\theta_{max} = 100°$ were collected. After the intensity data were corrected for Lorentz-polarization factors and absorption effects (ψ-scan method; North *et al.*, 1968), they were averaged in Laue symmetry mmm to give 692 independent reflections. Of these, independent reflections with $F_o \leq 3\sigma(F_o)$ were eliminated. Even if independent reflections had intensities of $F_o > 3\sigma(F_o)$ after averaging, those averaged from a data set of equivalent reflections including reflection(s) with $F_o \leq 3\sigma(F_o)$ were also discarded since these reflections were potentially affected by multiple scattering. Moreover, independent reflections with $(\sin \theta)/\lambda < 0.334$ Å^{-1} were eliminated to reduce secondary extinction effects and to avoid dependence on atomic charge as far as possible in the choice of atomic scattering factors. Finally, 412 independent reflections were used in the present refinement. Several correction models for the secondary extinction effects were attempted during the refinement, and the isotropic correction of Type II (Becker & Coppens, 1974a,b) with a Gaussian particle-size-distribution model yielded the best fit. The reliability indices converged to $R(F)$ = 0.0108 and $wR(F)$ = 0.0104 for 412 reflections, comparable to those of Hirai *et al.* (2009), and were dramatically improved in comparison with those of our previous report (Sugahara *et al.*, 2008). Crystal data, data collection and structure refinement details are summarized in Table 2.

References

Becker, P. J. & Coppens, P. (1974*a*). *Acta Cryst.* A**30**, 129–147.
Becker, P. J. & Coppens, P. (1974*b*). *Acta Cryst.* A**30**, 148–153.
Dowty, E. (2000). *ATOMS for Windows*. Shape Software, Kingsport, Tennessee, USA.
Hirai, S., Welch, M. D., Aguado, F. & Redfern, S. A. T. (2009). *Z. Kristallogr.* **224**, 345–350.
Iitaka, T., Hirose, K., Kawamura, K. & Murakami, M. (2004). *Nature*, **430**, 442–445.
Kojitani, H., Shirako, Y. & Akaogi, M. (2007). *Phys. Earth Planet. Inter.* **165**, 127–134.
Mao, W. L., Shen, G., Prakapenka, V. B., Meng, Y., Campbell, A. J., Heinz, D. L., Shu, J., Hemley, R. J. & Mao, H.-K. (2004). *Proc. Natl Acad. Sci. USA*, **101**, 15867–15869.
McDaniel, C. L. & Schneider, S. J. (1972). *J. Solid State Chem.* **4**, 275–280.
Murakami, M., Hirose, K., Kawamura, K., Sata, N. & Ohishi, Y. (2004). *Science*, **304**, 855–858.
Niwa, K., Yagi, T., Ohgushi, K., Merkel, S., Miyajima, N. & Kikegawa, T. (2007). *Phys. Chem. Miner.* **34**, 679–686.
North, A. C. T., Phillips, D. C. & Mathews, F. S. (1968). *Acta Cryst.* A**24**, 351–359.
Oganov, A. R. & Ono, S. (2004). *Nature*, **430**, 445–448.
Ono, S. & Oganov, A. R. (2005). *Earth Planet. Sci. Lett.* **236**, 914–932.

Rigaku (1999). *WinAFC*. Rigaku Corporation, Tokyo, Japan.

Rodi, F. & Babel, D. (1965). *Z. Anorg. Allg. Chem.* **336**, 17–23.

Sasaki, S. (1987). *RADY*. National Laboratory for High Energy Physics, Japan.

Shieh, S. R., Duffy, T. S., Kubo, A., Shen, G., Prakapenka, V. B., Sata, N., Hirose, K. & Ohishi, Y. (2006). *Proc. Natl Acad. Sci. USA*, **103**, 3039–3043.

Sugahara, M., Yoshiasa, A., Yoneda, A., Hashimoto, T., Sakai, S., Okube, M., Nakatsuka, A. & Ohtaka, O. (2008). *Am. Mineral.* **93**, 1148–1152.

Tateno, S., Hirose, K., Sata, N. & Ohishi, Y. (2010). *Phys. Earth Planet. Inter.* **181**, 54–59.

Tsuchiya, T. & Tsuchiya, J. (2007). *Phys. Rev. B*, **76**, 144119.

Tsuchiya, T., Tsuchiya, J., Umemoto, K. & Wentzcovitch, R. M. (2004). *Earth Planet. Sci. Lett.* **224**, 241–248.

Wentzcovitch, R. M., Tsuchiya, T. & Tsuchiya, J. (2006). *Proc. Natl Acad. Sci. USA*, **103**, 543–546.

Westrip, S. P. (2010). *J. Appl. Cryst.* **43**, 920–925.

Yamaura, K., Shirako, Y., Kojitani, H., Arai, M., Young, D. P., Akaogi, M., Nakashima, M., Katsumata, T., Inaguma, Y. & Takayama-Muromachi, E. (2009). *J. Am. Chem. Soc.* **131**, 2722–2726.

Yoneda, A., Fukui, H., Xu, F., Nakatsuka, A., Yoshiasa, A., Seto, Y., Ono, K., Tsutsui, S., Uchiyama, H. & Baron, A. Q. R. (2014). *Nat. Comms*, **5**, doi: 10.1038/ncomms4453.

supporting information

Crystal structure of post-perovskite-type CaIrO₃ reinvestigated: new insights into atomic thermal vibration behaviors

Akihiko Nakatsuka, Kazumasa Sugiyama, Akira Yoneda, Keiko Fujiwara and Akira Yoshiasa

Computing details

Data collection: *WinAFC* (Rigaku, 1999); cell refinement: *WinAFC* (Rigaku, 1999); data reduction: *RADY* (Sasaki, 1987); program(s) used to solve structure: coordinates taken from a previous refinement; program(s) used to refine structure: *RADY* (Sasaki, 1987); molecular graphics: *ATOMS for Windows* (Dowty, 2000); software used to prepare material for publication: *publCIF* (Westrip, 2010).

Calcium iridium(IV) trioxide

Crystal data

$CaIrO_3$	$F(000) = 484$
$M_r = 280.30$	$D_x = 8.214$ Mg m^{-3}
Orthorhombic, *Cmcm*	Mo $K\alpha$ radiation, $\lambda = 0.71069$ Å
Hall symbol: -C 2c 2	Cell parameters from 25 reflections
$a = 3.1466$ (5) Å	$\theta = 22.5–25.0°$
$b = 9.8690$ (16) Å	$\mu = 61.02$ mm^{-1}
$c = 7.3019$ (5) Å	$T = 298$ K
$V = 226.75$ (6) Å^3	Needle, dark reddish-brown
$Z = 4$	$0.20 \times 0.01 \times 0.01$ mm

Data collection

Rigaku AFC7R diffractometer	438 reflections with $F > 3.0\sigma(F)$
$\omega–2\theta$ scans	$R_{int} = 0.019$
Absorption correction: ψ scan (North *et al.*, 1968)	$\theta_{max} = 50.0°$
	$h = 0 \rightarrow 6$
	$k = -21 \rightarrow 21$
$T_{min} = 0.486$, $T_{max} = 0.543$	$l = -15 \rightarrow 15$
2593 measured reflections	3 standard reflections every 150 reflections
692 independent reflections	intensity decay: none

Refinement

Refinement on F	Weighting scheme based on measured s.u.'s $w = 1/\sigma^2(F)$
$R[F^2 > 2\sigma(F^2)] = 0.019$	
$wR(F^2) = 0.021$	$(\Delta/\sigma)_{max} = 0.0003$
$S = 1.56$	$\Delta\rho_{max} = 1.21$ e Å^{-3}
412 reflections	$\Delta\rho_{min} = -1.89$ e Å^{-3}
20 parameters	Extinction correction: isotropic Type II (Becker & Coppens, 1974*a,b*)
	Extinction coefficient: 1.50E4 (5)

Fractional atomic coordinates and isotropic or equivalent isotropic displacement parameters (Å²)

	x	*y*	*z*	U_{iso}*/U_{eq}
Ca	0.0000	0.7502 (1)	0.2500	0.0060 (2)
Ir	0.0000	0.0000	0.0000	0.00340 (5)
O1	0.0000	0.0756 (4)	0.2500	0.0065 (11)
O2	0.0000	0.3724 (3)	0.4495 (3)	0.0059 (7)

Atomic displacement parameters (Å²)

	U^{11}	U^{22}	U^{33}	U^{12}	U^{13}	U^{23}
Ca	0.0065 (3)	0.0055 (3)	0.0058 (3)	0.0000	0.0000	0.0000
Ir	0.00387 (6)	0.00317 (5)	0.00317 (5)	0.0000	0.0000	0.00001 (10)
O1	0.0084 (13)	0.0067 (12)	0.0045 (10)	0.0000	0.0000	0.0000
O2	0.0064 (9)	0.0054 (8)	0.0058 (7)	0.0000	0.0000	−0.0007 (6)

Geometric parameters (Å, º)

Ca—O1[i]	2.333 (3)	Ir—Ir[xxv]	3.6510 (3)
Ca—O1[ii]	2.333 (3)	O1—Ir	1.9722 (15)
Ca—O2[i]	2.460 (2)	O1—Ir[xxv]	1.9722 (15)
Ca—O2[ii]	2.460 (2)	O1—Ca[xxiii]	2.333 (3)
Ca—O2[iii]	2.460 (2)	O1—Ca[xxiv]	2.333 (3)
Ca—O2[iv]	2.460 (2)	O1—O1[xii]	3.1466 (5)
Ca—O2[v]	2.506 (3)	O1—O1[xiii]	3.1466 (5)
Ca—O2[vi]	2.506 (3)	O1—O1[vii]	3.944 (3)
Ir—O1	1.9722 (15)	O1—O1[xxv]	3.944 (3)
Ir—O1[vii]	1.9722 (15)	O1—O2[viii]	2.748 (2)
Ir—O2[viii]	2.0488 (18)	O1—O2[ix]	2.748 (2)
Ir—O2[ix]	2.0488 (18)	O1—O2[xxvi]	2.748 (2)
Ir—O2[x]	2.0488 (18)	O1—O2[xxvii]	2.748 (2)
Ir—O2[xi]	2.0488 (18)	O1—O2[xxiii]	2.936 (3)
Ca—Ca[xii]	3.1466 (5)	O1—O2[xxiv]	2.936 (3)
Ca—Ca[xiii]	3.1466 (5)	O1—O2[x]	2.936 (3)
Ca—Ca[xiv]	3.9755 (3)	O1—O2[xi]	2.936 (3)
Ca—Ca[xv]	3.9755 (3)	O1—O2[xxviii]	3.271 (4)
Ca—Ca[xvi]	3.9755 (3)	O1—O2	3.271 (4)
Ca—Ca[xvii]	3.9755 (3)	O2—Ir[xx]	2.0488 (18)
Ca—Ir[xviii]	3.0678 (9)	O2—Ir[xxi]	2.0488 (18)
Ca—Ir[xix]	3.0678 (9)	O2—Ca[xxiii]	2.460 (2)
Ca—Ir[i]	3.4501 (8)	O2—Ca[xxiv]	2.460 (2)
Ca—Ir[ii]	3.4501 (8)	O2—Ca[xix]	2.506 (3)
Ca—Ir[xx]	3.4501 (8)	O2—O1[xx]	2.748 (2)
Ca—Ir[xxi]	3.4501 (8)	O2—O1[xxi]	2.748 (2)
Ir—Ca[xxii]	3.0678 (9)	O2—O1[i]	2.936 (3)
Ir—Ca[vi]	3.0678 (9)	O2—O1[ii]	2.936 (3)
Ir—Ca[xxiii]	3.4501 (8)	O2—O1	3.271 (4)
Ir—Ca[xxiv]	3.4501 (8)	O2—O2[v]	2.625 (5)

Ir—Ca^{viii}	3.4501 (8)	O2—O2^{xxviii}	2.913 (5)
Ir—Ca^{ix}	3.4501 (8)	O2—O2^{xxvi}	2.976 (5)
Ir—Ir^{xii}	3.1466 (5)	O2—O2^{xxvii}	2.976 (5)
Ir—Ir^{xiii}	3.1466 (5)	O2—O2^{xii}	3.1466 (5)
Ir—Ir^{vii}	3.6510 (3)	O2—O2^{xiii}	3.1466 (5)
O1^{i}—Ca—O1^{ii}	84.82 (13)	O2^{vi}—Ca—O2^{iii}	73.63 (9)
O1^{i}—Ca—O2^{i}	86.02 (7)	O2^{vi}—Ca—O2^{iv}	73.63 (9)
O1^{i}—Ca—O2^{ii}	142.50 (6)	O2^{vi}—Ca—O2^{v}	122.28 (13)
O1^{i}—Ca—O2^{vi}	69.12 (5)	O2^{iii}—Ca—O2^{iv}	79.52 (8)
O1^{i}—Ca—O2^{iii}	86.02 (7)	O2^{iii}—Ca—O2^{v}	139.04 (5)
O1^{i}—Ca—O2^{iv}	142.50 (6)	O2^{iv}—Ca—O2^{v}	139.04 (5)
O1^{i}—Ca—O2^{v}	69.12 (5)	O1—Ir—O1^{vii}	180.00
O1^{ii}—Ca—O2^{i}	142.50 (6)	O1—Ir—O2^{viii}	86.22 (10)
O1^{ii}—Ca—O2^{ii}	86.02 (7)	O1—Ir—O2^{ix}	86.22 (10)
O1^{ii}—Ca—O2^{vi}	69.12 (5)	O1—Ir—O2^{x}	93.78 (10)
O1^{ii}—Ca—O2^{iii}	142.50 (6)	O1—Ir—O2^{xi}	93.78 (10)
O1^{ii}—Ca—O2^{iv}	86.02 (7)	O1^{vii}—Ir—O2^{viii}	93.78 (10)
O1^{ii}—Ca—O2^{v}	69.12 (5)	O1^{vii}—Ir—O2^{ix}	93.78 (10)
O2^{i}—Ca—O2^{ii}	79.52 (8)	O1^{vii}—Ir—O2^{x}	86.22 (10)
O2^{i}—Ca—O2^{vi}	139.04 (5)	O1^{vii}—Ir—O2^{xi}	86.22 (10)
O2^{i}—Ca—O2^{iii}	72.61 (10)	O2^{viii}—Ir—O2^{ix}	100.33 (12)
O2^{i}—Ca—O2^{iv}	121.28 (13)	O2^{viii}—Ir—O2^{x}	79.67 (12)
O2^{i}—Ca—O2^{v}	73.63 (9)	O2^{viii}—Ir—O2^{xi}	179.97
O2^{ii}—Ca—O2^{vi}	139.04 (5)	O2^{ix}—Ir—O2^{x}	179.97
O2^{ii}—Ca—O2^{iii}	121.28 (13)	O2^{ix}—Ir—O2^{xi}	79.67 (12)
O2^{ii}—Ca—O2^{iv}	72.61 (10)	O2^{x}—Ir—O2^{xi}	100.33 (12)
O2^{ii}—Ca—O2^{v}	73.63 (9)		

Symmetry codes: (i) $x-1/2, y+1/2, z$; (ii) $x+1/2, y+1/2, z$; (iii) $-x-1/2, y+1/2, -z+1/2$; (iv) $-x+1/2, y+1/2, -z+1/2$; (v) $x, -y+1, -z+1$; (vi) $-x, -y+1, z-1/2$; (vii) $-x, -y, z-1/2$; (viii) $-x-1/2, -y+1/2, z-1/2$; (ix) $-x+1/2, -y+1/2, z-1/2$; (x) $-x-1/2, y-1/2, -z+1/2$; (xi) $-x+1/2, y-1/2, -z+1/2$; (xii) $x-1, y, z$; (xiii) $x+1, y, z$; (xiv) $-x-1/2, -y+3/2, z-1/2$; (xv) $-x-1/2, -y+3/2, z+1/2$; (xvi) $-x+1/2, -y+3/2, z-1/2$; (xvii) $-x+1/2, -y+3/2, z+1/2$; (xviii) $x, y+1, z$; (xix) $-x, -y+1, z+1/2$; (xx) $-x-1/2, -y+1/2, z+1/2$; (xxi) $-x+1/2, -y+1/2, z+1/2$; (xxii) $x, y-1, z$; (xxiii) $x-1/2, y-1/2, z$; (xxiv) $x+1/2, y-1/2, z$; (xxv) $-x, -y, z+1/2$; (xxvi) $x-1/2, -y+1/2, -z+1$; (xxvii) $x+1/2, -y+1/2, -z+1$; (xxviii) $-x, y, -z+1/2$.